

Gripper Keypose and Object Pointflow as Interfaces for Bimanual Robotic Manipulation

Author Names Omitted for Anonymous Review. Paper-ID [434]

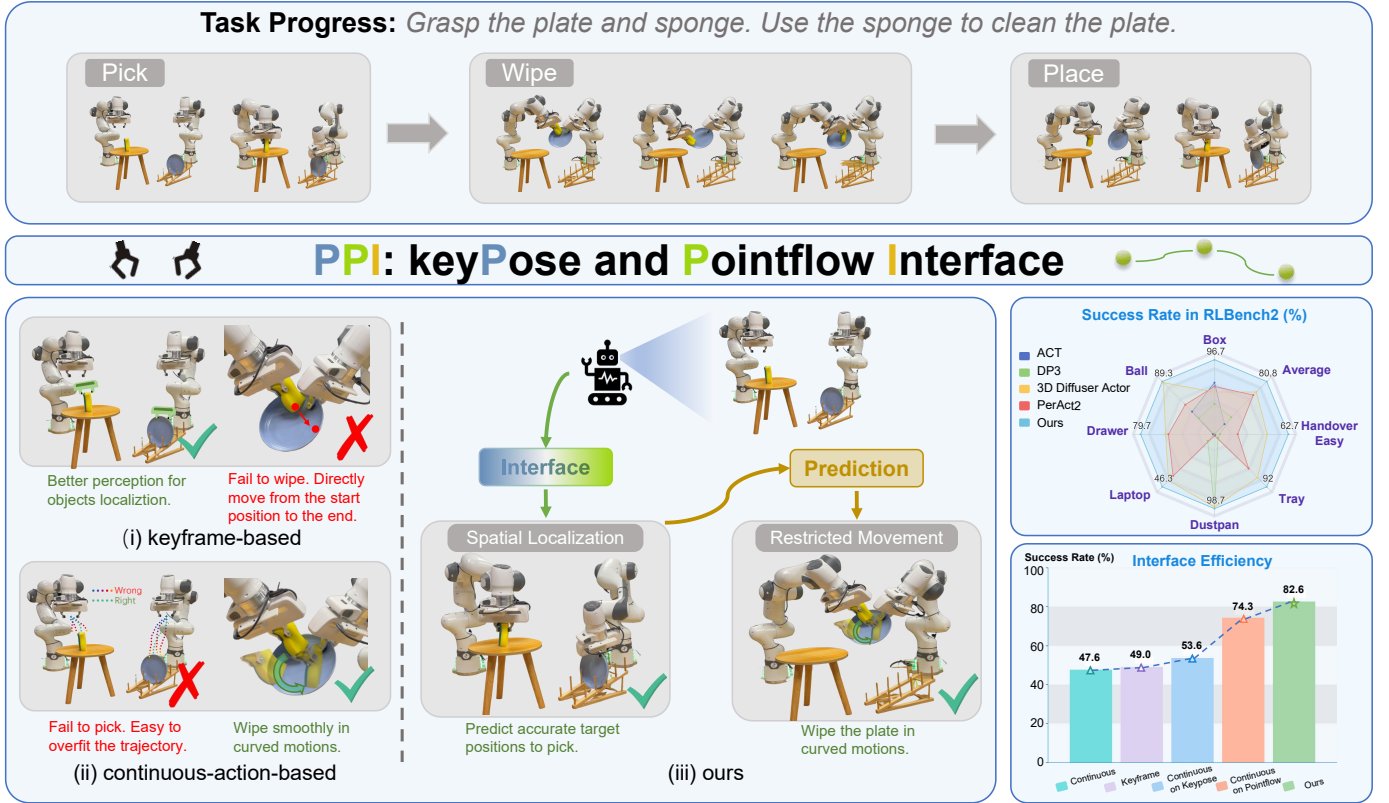


Fig. 1: In contrast to (i) keyframe-based policies, which excel in spatial localization but struggle with movement restrictions(e.g., curved motion and collision-free actions), and (ii) continuous-action-based policies, which accommodate diverse trajectories but lack strong perception, we introduce a continuous action policy that incorporates two interfaces: target gripper poses and object pointflow, balancing task diversity with spatial awareness. Our model, PPI, surpasses previous states of the art and consistently outperforms its ablated variants.

Abstract—Bimanual manipulation is a challenging yet crucial robotic capability, demanding precise spatial localization and versatile motion trajectories, which pose significant challenges to existing approaches. Existing approaches fall into two categories: keyframe-based strategies, which predict gripper poses in keyframes and execute them via motion planners, and continuous control methods, which estimate actions sequentially at each timestep. The keyframe-based method lacks inter-frame supervision, struggling to perform consistently or execute curved motions, while the continuous method suffers from weaker spatial perception. To address these issues, this paper introduces an end-to-end framework PPI (keyPose and Pointflow Interface), which integrates the prediction of target gripper poses and object pointflow with the continuous actions estimation. These interfaces enable the model to effectively attend to the target manipulation area, while the overall framework guides diverse and collision-free trajectories. By combining interface predictions with continuous actions estimation, PPI demonstrates superior performance in diverse bimanual manipulation tasks, providing

enhanced spatial localization and satisfying flexibility in handling movement restrictions. In extensive evaluations, PPI significantly outperforms prior methods in both simulated and real-world experiments, achieving the state-of-the-art performance on the RLBench2 simulation benchmark and across four challenging real-world tasks. Notably, PPI exhibits strong stability, high precision, and remarkable generalization capabilities in real-world scenarios. Code and models will be released.

I. INTRODUCTION

Endowing robots with dexterous bimanual skills similar to humans has become a main focus in robotic manipulation [3, 6, 14, 34, 36]. Recent efforts primarily fall into two categories: one focuses on “keyframe”, like [9, 13], which predict actions in the reference frames and execute predictions via Inverse Kinematics (IK) solvers and motion planners [31]. The other emphasizes “continuous” and perform naive behavior cloning at each time step. For example, ACT [48]

and RDT [18] learn RGB-based manipulation policies from multiple cameras, while DP3 [46] integrate 3D scene-level representations into a diffusion policy.

However, due to the temporal granularity of action prediction, the keyframe-based methods predicts actions only at few keyframes. This sparse supervision encourages the model to focus more on local features, enhancing spatial perception. Nevertheless, for tasks involving restricted movements (e.g., wiping a plate, which requires curved trajectories), keyframes are difficult to define and the motion planner [31, 30] tends to output near straight-line paths, making such tasks challenging to accomplish. For continuous-based methods, they are generally applicable to a wide range of tasks. Whereas, since they rely on naive behavior cloning with dense supervision on actions, the model tends to “take shortcuts” by overfitting to seen trajectories (e.g., proprioception). This results in weaker spatial perception capabilities. Therefore, implementing diverse general bimanual tasks while preserving strong perceptual capabilities remains a critical challenge.

To this end, this paper presents a simple yet effective end-to-end interface-based continuous policy that integrates the strengths of previous approaches. As illustrated in Figure 1, our model predicts continuous actions conditioned on two key interfaces: the target gripper keypose and object pointflow. These interfaces enable the model to capture fine-grained spatial features and comprehensively model the interaction between the robot and the object. We implement a diffusion transformer [13, 46] to process both interfaces, naming our approach PPI. By distilling spatial knowledge from these interfaces, PPI strikes a balance between handling diverse tasks and maintaining strong perception capabilities. Leveraging a unidirectional attention mask within the transformer, PPI progressively infers actions and is trained in an end-to-end manner.

We conduct extensive experiments on both simulation and real-world benchmarks. On the bimanual manipulation benchmark RLBenchmark2 [9], our method achieves a 16.1% higher success rate across seven representative tasks compared to state-of-the-art baselines. We further provide comprehensive visualizations to validate the effectiveness of the two interfaces. Additionally, we evaluate our approach on four challenging real-world tasks [42], demonstrating superior performance in long-horizon task execution, generalization to unseen objects, robustness to lighting variations, and resilience against visual distractions.

Our contributions are summarized as follows:

- We present a novel framework that utilizes keyframe information to guide continuous action generation, improving flexibility in addressing movement constraints.
- We propose two effective interfaces—target gripper poses and object pointflow to boost spatial localization and generalization.
- We provide comprehensive analyses to validate the power of two interfaces. We achieve the state-of-the-art performance on a bimanual simulation benchmark and demonstrate strong robustness, effectiveness, and generalization

in real-world long-horizon tasks.

II. RELATED WORKS

A. Behavior Cloning in General Bimanual Manipulation Tasks

Current behavior cloning methods for general bimanual manipulation tasks can be broadly classified into two categories. The first category involves keyframe-based strategies [9, 16, 8], where keyframe representations [2, 49, 33] are learned and executed through motion planners. Approaches such as PerAct2 [9] and VoxAct-B [16] predict target gripper poses in a reference frame using voxel-based representations. Additionally, DualAfford [49] learns collaborative object-centric affordances and applies heuristic policies for execution. However, these methods rely on rule-based keyframe split and motion planners, which limits their ability to handle tasks that require irregular motion trajectories (e.g., dishwashing) or strict temporal coordination (e.g., tray lifting). The second category involves continuous control, where actions are estimated sequentially at each time step. For instance, ACT [48] uses an action-chunking transformer to predict actions in an end-to-end manner, while RDT [18] employs a diffusion-based transformer, pre-trained on large robot datasets and fine-tuned on self-collected bimanual data. BiKC [44], is an RGB-based hierarchical framework consisting of a high-level keypose predictor and a low-level trajectory generator. Some works also extend single-arm manipulation policies [4, 46] to the bimanual setting. In contrast to these continuous control approaches, our method integrates a 3D semantic neural field [37, 38] and predicts pointflow as an additional interface, thereby enhancing spatial localization capabilities.

B. Flow-based Methods in Robotic Manipulation

Robot manipulation policies have utilized either 2D pixel-level motion [12, 32, 25, 41] or 3D point-level flow [47, 20, 5] for object interaction. In 2D flow-based approaches, recent pixel-tracking algorithms [12] estimate motion flows in robotic video data. Track2Act [1] integrates a residual strategy atop heuristic and flow-based policies, while ATM [40] learns a flow-conditioned behavior cloning policy trained on self-collected, in-domain data. Im2Flow2Act [43] further introduces a data-efficient, fully autonomous flow-conditioned policy, leveraging task-agnostic datasets for one-shot real-world transfer. Unlike these 2D methods, PPI leverages 3D point-level flow, enhancing spatial localization and enables more accurate manipulation. This approach builds upon prior work in 3D flow-based policies, which have shown promising results in articulated object manipulation [7], tool use [26, 22], and general skill learning [45]. However, these methods typically rely on manually designed or heuristic policies during execution after estimating 3D flow. In contrast, PPI introduces an end-to-end manipulation policy, eliminating the need for heuristic post-processing.

III. METHOD

In this section, we describe PPI in detail. We begin with a brief problem formulation (Section III-A). Next, we discuss

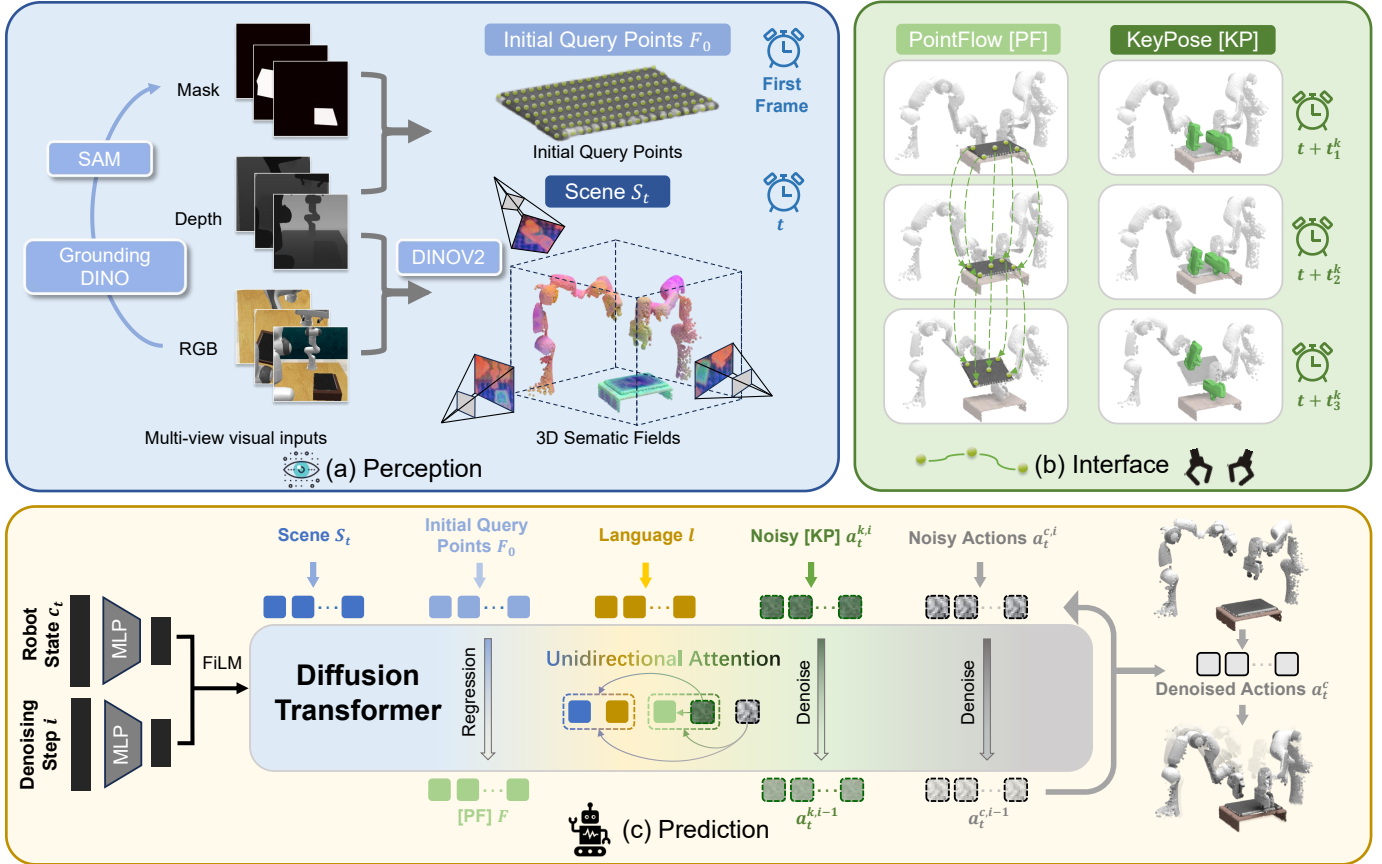


Fig. 2: **Overview of PPI.** (a) **Perception.** We first construct a 3D semantic neural field S_t and sample initial query points F_0 for pointflow prediction. (b) **Interface.** Next, we define two intermediate interfaces: target gripper poses a_t^k and object pointflow F . (c) **Prediction.** Finally, a diffusion transformer incorporates robot proprio tokens c_t , scene tokens S_t , language tokens l , pointflow query tokens F_0 and action tokens a_t^k and a_t^c with gaussian noise. Using a carefully designed unidirectional attention mask, the model progressively denoises action predictions conditioned on the interfaces.

the perception module (Section III-B) in PPI, involving the construction of 3D semantic neural field and initial query points. Subsequently, we elaborate on the key interface designs—Pointflow and Keypose (Section III-C), enhancing PPI spatial localization capabilities. Then, we illustrate the action prediction module (Section III-D), which is a diffusion-based transformer with a unidirectional attention mask. Finally, we provide a detailed implementation details during training and inference phases (Section III-E).

A. Problem Formulation

At time step t , PPI takes inputs as the language instruction l and RGBD images \mathcal{I} from K cameras, and outputs a sequence of h^c continuous actions $a_t^c = \{a_{t:t+h^c}\}$, where each action a_t represents the target gripper pose and openness for both the left and right grippers. Crucially, PPI incorporates two intermediate **interfaces** at **keyframe** timesteps as additional conditions for action prediction. The **keyframe** t^k are defined as turning points in the trajectory where there are significant changes in the grippers' openness and the arms' joint states [11, 27]. For the **interfaces**, the first specifies the target gripper pose

at the subsequent h^k keyframes: $a_t^k = \{a_{t_i^k}\}_{i=1}^{h^k}$. The second interface defines the positions of N_q spatial query points at the next h^k keyframes: $F \in \mathbb{R}^{h^k \times N_q \times 3}$. At each keyframe timestep t_i^k , the positions of the N_d points are denoted as $F_{t_i^k} \in \mathbb{R}^{N_d \times 3}$, with initial positions at the first frame given by $F_0 \in \mathbb{R}^{N_d \times 3}$.

B. Perception

3D Scene Representation. As is seen in Figure 2(a), we represent the scene using 3D semantic fields, focusing on both geometric and semantically meaningful regions. We begin by preprocessing the raw point clouds through cropping and downsampling. For each sampled 3D point, we project it onto 2D RGB images from multiple camera viewpoints to extract pixel-wise semantic features using the DINOV2 [19] model. We fuse these features through a weighted sum, where the weights are determined by the point's distance from the projected surface.

To mitigate the computational burden of numerous scene tokens in the transformer backbone, we downsample scene points while preserving their geometric and semantic infor-

mation. We use a PointNet++ dense encoder [23] to obtain a compact scene representation $S_t \in \mathbb{R}^{N_s \times (3+D)}$, where each of the N_s points encodes spatial coordinates and a D-dimensional fused semantic feature. This compressed representation retains key geometric and semantic details while enhancing local point relationships through PointNet++’s set abstraction.

Initial Query Points Sampling. Instead of directly learning the pointflow distribution $p(F)$, we choose to approximate the conditional distribution $p(F|F_0)$, where F_0 represents the initial query points sampled from the manipulated object at the first frame. This approach shifts the model’s focus from inferring global absolute coordinates to capturing overall object motion. Consequently, even when the object position is out of distribution, PPI can estimate pointflow accurately and robustly, demonstrating improved generalization.

To get the initial query points F_0 , we randomly sample N_q query points from the object to be manipulated at the beginning of the task. We use the Grounding DINO model [17] to obtain a bounding box from the language prompt and image, then input the bounding box into the SAM model [15] to generate the object mask. We obtain the 3D coordinates $F_0 \in \mathbb{R}^{N_q \times 3}$ of the N_q pixels sampled from the mask. In practice, we find that $N_q = 200$ points are sufficient for all tasks, both in simulation and the real world. It is worth noting that in each episode, we will only perform this operation once.

C. Interface

Target Gripper Poses. We predict target gripper poses at keyframe timesteps as explicit action goals to better guide continuous action generation. To supervise the target gripper poses, we first use a heuristic algorithm to identify the keyframe timesteps in the trajectory. Once a keyframe t_i^k is established, its corresponding action label $a_{t_i^k}$ can be directly retrieved. If there are fewer keyframes remaining after the current timestep than h^k , we pad the sequence by repeating the action of the last keyframe.

Object Pointflow. A key challenge in obtaining ground truth labels for pointflow is the inevitable occlusion that occurs when the object moves or is manipulated. We address this challenge by leveraging the object’s 6D pose to track the real-time points’ positions. In simulation, we obtain the ground truth 6D pose label of rigid objects from the RL Bench2 [9] dataset, while in the real world, we estimate it using BundleSDF [39] and Foundation Pose [2]. Given the object’s 6D pose at the first and each keyframe timestep, we transform the query points from the first frame F_0 into the object’s coordinate frame and then back into world coordinates, yielding their keyframe positions $F_{t_i^k} \in \mathbb{R}^{N \times 3}$, which serve as the ground truth for pointflow supervision. Here real-time object 6D pose estimation is not required during inference. Overall, object pointflow along with target gripper poses effectively model the interaction between the object and the robot.

D. Prediction

Observation Encoder. PPI processes four types of inputs: the 3D semantic neural field S_t , the language instruction ℓ ,

the robot states c_t and the initial positions of point queries F_0 . The language is encoded using a CLIP text tokenizer [24] and projected into a latent space via a three-layer MLP. Similarly, the robot states and point queries are projected into the latent space through a three-layer MLP.

Diffusion Transformer. The backbone of the prediction module builds upon a diffusion transformer. At the time step t and denoising step i , let $a_t^{k,i}$ and $a_t^{c,i}$ be the keyframe action a_t^k and continuous action a_t^c with noise. The transformer incorporates the scene tokens S_t , language tokens ℓ , query points tokens F_0 and noised action tokens $a_t^{k,i}$ and $a_t^{c,i}$. Outputs are supervised by gaussian noise ϵ_k^i , ϵ_c^i via DDPM [10] training and ground truth pointflow F via direct regression.

Notably, we design a unidirectional attention mask that leverages the interfaces to bridge the gap between input and output modalities. As shown in Figure 2 (c), all pointflow and action tokens attend to the scene and language tokens, integrating spatial and semantic knowledge. Moreover, the noised keyframe action token $a_t^{k,i}$ attends to the pointflow token, aiming to extract additional object-level features. The final continuous action token $a_t^{c,i}$ attends to all the previous tokens, not only distilling regular scene-level features but also fully utilizing the local and detailed features contained in the interfaces.

We apply relative attention, as introduced in previous work [13], between point flow tokens F , keyframe action tokens $a_t^{k,i}$, continuous action tokens $a_t^{c,i}$, and scene point cloud tokens S_t , enabling the encoding of relative 3D positional information in the attention layers. This relative attention relies on the relative 3D positions of features and is implemented using rotary positional embeddings [29]. For language instructions ℓ , we use regular cross and self-attention. The robot’s proprioception c_t and denoising timesteps i affect the attention through Feature-wise Linear Modulation(FiLM) [21].

E. Implementation Details

Training. For the PPI network ϵ_θ , the continuous action loss \mathcal{L}_c , the keyframe action loss \mathcal{L}_k , and the pointflow prediction loss \mathcal{L}_F are computed via L_1 loss.

$$\begin{aligned}\mathcal{L}_c &= \|\epsilon_\theta(S_t, F_0, \ell, c_t, a_t^{c,i}, i) - \epsilon_c^i\| \\ \mathcal{L}_k &= \|\epsilon_\theta(S_t, F_0, \ell, c_t, a_t^{k,i}, i) - \epsilon_k^i\| \\ \mathcal{L}_F &= \|\epsilon_\theta(S_t, F_0, \ell, c_t) - F\|\end{aligned}$$

The overall training loss is:

$$\mathcal{L}_\theta = w_1 \mathcal{L}_c + w_2 \mathcal{L}_k + w_3 \mathcal{L}_F$$

where w_1 , w_2 , and w_3 are hyperparameters set to 0.05, 0.05, and 1, respectively. We use DDPM with 1000 training timesteps for noise scheduling in all experiments. We train 500 epochs for tasks from RL Bench2 benchmark and 5000 epochs in real-world tasks, with a batch size of 128 and learning rate of 1e-4 with a cosine decay learning rate scheduler. For tasks involving 100 episodes, each with 150-250 timesteps, we train the model using eight A100 GPUs for approximately 20 hours,



Fig. 3: Task process visualizations in four real-world tasks.

and use the checkpoint with the lowest average validation loss for evaluation.

Inference. We begin by sampling 200 points on objects as query points at the first timestep. Then at each timestep t , we draw random initial continuous action samples a_t^c and keyframe action samples a_t^k from a Gaussian distribution and denoise 1000 steps with DDPM in simulation tasks and 20 steps with DDIM[28] for real-world tasks. In practice, we predict 50 continuous actions and 4 keyframe actions and pointflow.

IV. REAL-WORLD EXPERIMENTS

We carefully design four real-world tasks with high localization demands and motion constraints to evaluate PPI’s capabilities in: (1) Effectiveness in long-horizon tasks. (2) Robustness under high-intensity disturbances in objects and environments.

A. Real-world Experiments Setup

Benchmark. We evaluate our method on two Franka Research 3 robots across four tasks in two distinct scenarios (Figure 4). Each scene is equipped with two Eye-on-Hand and one Eye-on-Base RealSense D435i cameras. In the first desktop environment, we test three long-horizon tasks requiring high localization accuracy and curved motion execution. In the second shelf scenario, we employ Robotiq-2f-85 grippers as end-effectors for the final task. Below, we briefly outline the process for each of the four tasks (Figure 3), with further details provided in the Appendix.

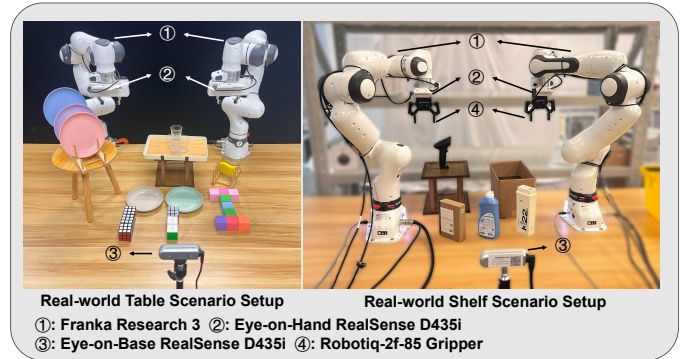


Fig. 4: Two real-world setups.

- 1) **Carry the Tray.** Both arms must collaboratively lift a tray stacked with cups or other objects from a lower platform and steadily transfer it to a small table. This task evaluates the ability to precisely locate the tray’s centerline and maintain stable, coordinated movements throughout the process.
- 2) **Handover and Insert the Plate.** The right arm picks up the plate and hands it over to the left arm, which then inserts it into an available slot in the rack. This task tests temporal coordination during handover and precise spatial perception.
- 3) **Wipe the Plate.** Each arm picks up the sponge and the plate, respectively, and uses the sponge to wipe the plate. After wiping, both objects are returned to their original positions. This task evaluates the ability

TABLE I: Real-world main results. We evaluate all the methods with 10 (settings) \times 3 (repeated trials) rollouts per task. Our method achieves better performances among all tasks than baselines. The best results are bolded.

Method	SR (%) ↑ / Loc-SR (%) ↑ / Normalized Score ↑				
	Avg. Success ↑	Carry the Tray	Handover and Insert the Plate	Wipe the Plate	Scan the Bottle
ACT	10.0 / 20.0 / 2.6	30.0 / 30.0 / 5.5	0.00 / 0.00 / 0.0	0.00 / 0.00 / 0.0	10.0 / 50.0 / 5.0
DP3	7.50 / 30.0 / 2.9	0.00 / 10.0 / 1.5	10.0 / 50.0 / 2.7	20.0 / 40.0 / 4.0	0.00 / 20.0 / 3.3
3D Diffuser Actor	0.00 / 67.5 / 4.4	0.00 / 70.0 / 4.5	0.00 / 100 / 6.0	0.00 / 50.0 / 3.5	0.00 / 50.0 / 3.8
Ours	52.5 / 90.0 / 8.0	50.0 / 100 / 7.5	40.0 / 100 / 7.7	70.0 / 70.0 / 8.3	50.0 / 90.0 / 8.5

to perform curved motions in interactive tasks.

- 4) **Scan the Bottle.** The right arm retrieves the bottle from the shelf, while the left arm picks up the scanner from the table to scan the bottle’s barcode. After scanning, the bottle is placed into a box. This task assesses 6-DoF picking in a more constrained spatial environment and the coordination between both arms.

Expert demonstrations. We constructed two isomorphic teleoperation devices GELLO [42] for the Franka Research 3 to collect expert demonstrations. We collected 50 demonstrations for the task “Carry the Tray” and 20 for other tasks. The limited number of training samples is intended to evaluate whether the policies achieve excellent spatial localization and perception of objects with minimal data.

Baselines. We implement an Action Chunking Transformer (ACT) [48] that predicts target joint positions from 2D RGB inputs. We also adapt DP3 [46] into a bimanual framework, which is a 3D point-cloud-based continuous control policy. Additionally, we reproduce the 3D Diffuser Actor [13], a keyframe-based diffusion policy utilizing 3D semantic fields.

Metrics. Each method is evaluated across 10 settings, with 3 trials per setting. Due to the long-horizon and complex nature of the tasks, we have established three key metrics: Success Rate (SR), Localization Success Rate (Loc-SR), and Normalized Score. The Success Rate (SR) is only assigned a value of 100% upon the successful completion of the entire task. Loc-SR will be recorded 100% if the robots perform well to find the object contact positions. Additionally, we divide each tasks into 3 or 4 intermediate stages, and the Score is progressively accumulated through the completion of individual intermediate stages. Given that the number of steps varies across these tasks, the score will be normalized to a scale of 10. The scoring criteria and other details are available in the Appendix.

B. Real-world Main Results

As shown in Table I, PPI outperforms all baselines across tasks. Compared to state-of-the-art methods, it achieves a 42.5% increase in average success rate (SR), a 22.5% improvement in localization success rate (Loc-SR), and a 3.6 point gain in Normalized Score. Compared to ACT, which relies on RGB inputs, PPI demonstrates superior Loc-SR and overall scores. As a single-frame observation algorithm, ACT struggles with tasks requiring repetitive trajectories (e.g., “Wipe the Plate”), whereas PPI integrates multistep proprioception, effectively leveraging historical information. Compared to DP3, a point-

cloud-based method prone to overfitting seen trajectories and susceptible to noise [35], PPI exhibits stronger localization ability and robustness to noised pointcloud. While 3D Diffuser Actor, a keyframe-based policy using semantic neural fields and heuristic action execution, performs well in Loc-SR and Normalized Score, it fails to account for collision constraints, leading to a lower SR. In contrast, PPI not only inherits the perception advantages of keyframe prediction but also effectively respects path constraints inherent in training demonstrations.

C. Real-world Generalization Tests

As shown in Table II-V and Figure 5-8, We introduce three types of generalizations to evaluate the generalizability and robustness: unseen objects to manipulated, different lighting backgrounds and interference from other objects. In each task, we select the setting where each method performed the best for generalization testing, and then we record the success rate, localization success rate, and normalized score. Each different generalization scenario has 3 trials. Details results are available in the Appendix.

TABLE II: Evaluation under object interference in Carry the Tray.

Method	Success / Localization / Normalized Score		
	Normal Setting	Rubik's Cubes	Colorful Cubes
ACT	✓/✓/ 10	✓/✓/ 10	✓/✓/ 10
DP3	X/✓/ 5.0	X/ X/ 2.5	X/✓/ 5.0
3D Diffuser Actor	X/✓/ 5.0	X/✓/ 5.0	X/ X/ 2.5
Ours	✓/✓/ 10	✓/✓/ 10	✓/✓/ 10

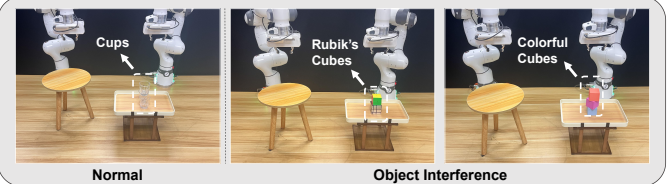


Fig. 5: Visualization under object interference in Carry the Tray.

In **Carry the Tray**, we replace the cups with Robik’s Cubes and colorful cubes to test robustness against **object interference**. These objects differ in size, color, and light transmittance, which not only affect RGB inputs but also alter depth, influencing 3D-based policies. Thanks to the two interfaces, particularly the pointflow, PPI focuses on key object-

related regions, such as the tray, without being distracted by other objects that could affect localization. Interestingly, two 3D-based baselines perform poorly, while the 2D-based ACT achieves better generalization. This suggests that although objects in this task have minimal impact at the pixel level in 2D images, they have a greater effect on the 3D scene representation.

TABLE III: Evaluation under different lightning backgrounds in Handover and Insert the Plate.

Method	Success / Localization / Normalized Score		
	Normal Setting	Dark Environment	Flickering Lighting Environment
ACT	X/ X/ 0.0	X/ X/ 0.0	X/ X/ 0.0
DP3	✓/ ✓/ 10	X/ X/ 6.7	✓/ ✓/ 10
3D Diffuser Actor	X/ ✓/ 6.7	X/ X/ 0.0	X/ X/ 0.0
Ours	✓/ ✓/ 10	✓/ ✓/ 10	✓/ ✓/ 10

Fig. 6: Visualization under different lightning backgrounds in Handover and Insert the Plate.

In **Handover and Insert the Plate**, we evaluate PPI's adaptability to varying **lighting conditions**. In dark and flashing environments, RGB-based information is severely affected. However, despite using color information as inputs, PPI's performance remains stable. This robustness probably stems from its reliance on pointflow and keypose, both derived mostly from the integration of semantic and positional features rather than pure color information. Meanwhile, DP3 maintains some success, likely due to its use of colorless point clouds.

TABLE IV: Evaluation under object interference in Wipe the Plate.

Method	Success / Localization / Normalized Score		
	Normal Setting	Colorful Cubes	Multi-plate
ACT	X/ X/ 0.0	X/ X/ 0.0	X/ X/ 0.0
DP3	✓/ ✓/ 10	X/ X/ 0.0	X/ X/ 0.0
3D Diffuser Actor	X/ ✓/ 5.0	X/ ✓/ 5.0	X/ ✓/ 5.0
Ours	✓/ ✓/ 10	✓/ ✓/ 10	✓/ ✓/ 7.5

Fig. 7: Visualization under object interference in Wipe the Plate.

In **Wipe the Plate**, we introduce **object interference** separately for the objects manipulated by each arm, leading to partial occlusions and various visual distractions. Despite this, only PPI maintains robust localization.

TABLE V: Evaluation under unseen objects in Scan the Bottle.

Method	Success / Localization / Normalized Score		
	Normal Setting	Box	Yogurt bottle
ACT	✓/ ✓/ 10	X/ X/ 2.5	X/ X/ 2.5
DP3	X/ ✓/ 7.5	X/ X/ 2.5	X/ X/ 2.5
3D Diffuser Actor	X/ ✓/ 5.0	X/ X/ 2.5	X/ X/ 2.5
Ours	✓/ ✓/ 10	X/ ✓/ 7.5	X/ ✓/ 7.5

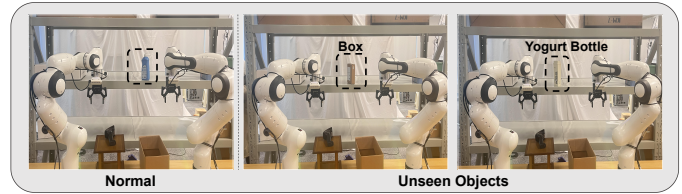


Fig. 8: Visualization under unseen objects in Scan the Bottle.

In **Scan the Bottle**, we evaluate our method's generalization to **unseen objects**. Notably, PPI enables zero-shot manipulation of new objects by adjusting GroundingDino's [17] prompt to obtain novel initial query points F_0 for pointflow prediction. A key factor in this outcome is that the conditional distribution $p(F|F_0)$ learned by PPI for predicting pointflow. This is driven by PPI's learned conditional distribution $p(F|F_0)$, which prioritizes object motion changes over absolute global coordinates $p(F)$. As a result, even when encountering novel rigid objects, PPI effectively estimates a rough object's relative transformations, enhancing task completion.

V. SIMULATION EXPERIMENTS

We evaluate our approach on seven tasks using the bimanual simulation benchmark RL Bench2 [9], aiming to address the following questions: (1) How well does PPI perform on complex bimanual tasks? (2) Are the proposed target gripper pose and object pointflow interfaces effective? (3) How do these interfaces learn scene features to enhance guidance for continuous action prediction?

A. Simulation Experiments Setup

Benchmark. RL Bench2 [9] is a bimanual manipulation benchmark built on CoppeliaSim, encompassing tasks with different levels of coupling, coordination, language instructions, and manipulation skills. We select seven representative and challenging tasks and regenerate the training data. The official dataset suffers from significant misalignment between training and evaluation, such as robot shadows present in the training set but absent during evaluation. Additionally, it lacks meta information for acquiring object pointflow.

Baselines. We use the same three baselines as in the real-world experiments: DP3, ACT, and 3D Diffuser Actor. Additionally, we include PerAct² [9], a state-of-the-art method

TABLE VI: Quantitative results on RL Bench2. For each task, we present the average performance of three checkpoints averaged over 100 rollouts. The metric “Avg. Success” measures the average success rate across seven tasks. PPI outperforms baselines with higher Avg. Success and better results on most tasks. The best results are bolded.

Method	Avg. Success ↑	Box	Ball	Drawer	Laptop	Dustpan	Tray	Handover Easy
ACT	15.4	67.0 ± 7.0	38.3 ± 10.0	1.7 ± 2.1	0.0 ± 0.0	0.0 ± 0.0	1.3 ± 1.5	0.0 ± 0.0
DP3	26.0	39.3 ± 3.1	27.0 ± 6.6	0.0 ± 0.0	6.0 ± 2.6	98.7 ± 0.6	6.3 ± 0.6	4.7 ± 1.5
3D Diffuser Actor	64.7	54.7 ± 3.8	87.3 ± 1.9	52.7 ± 14.1	40.7 ± 6.1	96.7 ± 2.6	76.0 ± 4.3	44.7 ± 3.3
PerAct ²	40.0	62.0 ± 26.2	50.0 ± 8.7	49.7 ± 16.6	36.7 ± 5.7	2.0 ± 3.5	60.0 ± 6.2	19.7 ± 6.0
Ours	80.8	96.7 ± 1.5	89.3 ± 1.5	79.7 ± 3.8	46.3 ± 1.2	98.7 ± 1.5	92.0 ± 1.0	62.7 ± 2.5

previously reported on RL Bench2. It employs a Perceiver architecture to voxelize 3D spaces and predict keyframe actions.

Metrics. Each method is evaluated across 100 rollouts per task with varying initial states for each tasks. We report both per-task and average success rates, with all performances computed from three different checkpoints.

B. Simulation Main Results

As shown in Table VI, PPI achieves an average success rate of 80.8%, significantly outperforming the baselines. Compared to ACT (2D-based algorithm), PPI leverages 3D semantic neural fields, and provides superior spatial perception. While both methods utilize 3D point clouds, PPI outperforms DP3 by 54% in success rate, demonstrating that PPI’s spatial information processing is more useful than DP3’s approach of encoding the entire scene into a single token.

Moreover, ACT and DP3, as continuous-action-based policies, underperforms keyframe-based policies like 3D Diffuser Actor and PerAct² by a margin of at least 10%. This disparity arises from keyframe-based methods offering more effective perception capabilities rather than overfitting to trajectories. By using keyposes as an interface, PPI integrates the spatial awareness of keyframe methods with semantic neural fields, achieving substantial improvements over continuous-action-based approaches.

Beyond that, keyframe-based policies like 3D Diffuser Actor and PerAct² fall behind our model in tasks with movement constraints, such as the lift tray task (which requires both hands to remain level) and the push box task (which involves continuously pushing). This is because our policy provides greater flexibility in managing such constraints, enabled by PPI’s supervision of continuous actions between keyframes. Additionally, in tasks demanding high spatial precision, such as object-picking tasks like Drawer and Handover Easy, our model significantly outperforms baselines. This advantage stems primarily from the use of object pointflow as an interface, which enhances localization accuracy.

C. Ablation Study

As shown in Table VII, we analyze the contributions of target gripper poses and object pointflow interfaces on RL Bench2 by comparing different ablated models at their best performance.

We begin by evaluating the vanilla keyframe and continuous baselines, which predict only keypose or continuous actions, respectively. In tasks requiring precise positioning, such as Handover Item and Lift Ball, the keyframe-based policy demonstrates superior localization. However, in tasks involving horizontal lifting (Lift Tray) or curved motion trajectories (Sweep to Dustpan), the continuous-based approach significantly outperforms the keyframe method. These results indicate that relying solely on either keyframe or continuous actions is insufficient for general manipulation tasks.

Next, we modify the continuous-based policy by incorporating target gripper keypose and object pointflow predictions (line 3 and 4 in Table VII). Conditioning on separate interfaces improves performance, likely due to the local spatial features they provide. Moreover, combining both interfaces yields further gains, highlighting the synergy between keypose and pointflow in enhancing performance on downstream tasks.

D. Visualization Analysis

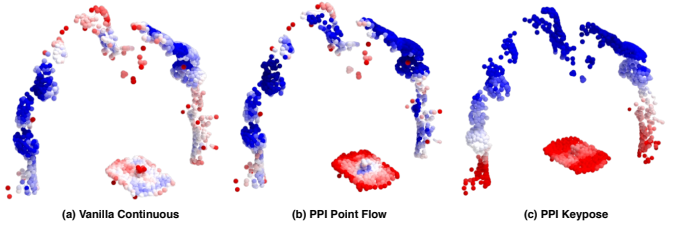


Fig. 9: Visualization of the attention weights of interface tokens. We use “Lift Tray” task on RL Bench2 as an example. The **red** area corresponds to larger attention weight, while the **blue** area corresponds to smaller attention weight. **Left:** The attention weights of continuous tokens to the 1024 scene tokens in the vanilla continuous-action-based policy. **Middle:** The attention weights of point flow tokens to the scene tokens in PPI. **Right:** The attention weights of keypose tokens in PPI.

In this section, we intuitively analyze how the proposed interfaces enhance localization accuracy and generalization to distractors and task-irrelevant backgrounds.

As shown in Figure 9, we visualize attention weights for our policy and the vanilla continuous-based policy in the “Lift Tray” task on RL Bench2. The left image reveals that in the continuous-based policy, action tokens fail to consistently

TABLE VII: **Ablation studies.** For all ablated models, we report best performance, while for PPI, we additionally present the average performance across three checkpoints. Overall, integrating both keypose and pointflow achieves the highest performance.

Method	Avg. Success ↑	Box	Ball	Drawer	Laptop	Dustpan	Tray	Handover	Easy
Continuous	47.6	84	24	41	0	98	82	4	
Keyframe	49.0	84	94	36	0	92	12	25	
Continuous on Keypose	53.6	71	81	29	1	99	86	8	
Continuous on Pointflow	74.3	92	77	84	29	99	89	50	
Ours (Best Ckpt)	82.6	98	91	84	47	100	93	65	
Ours (Averaged)	80.8	96.7	89.3	79.7	46.3	98.7	92.0	62.7	

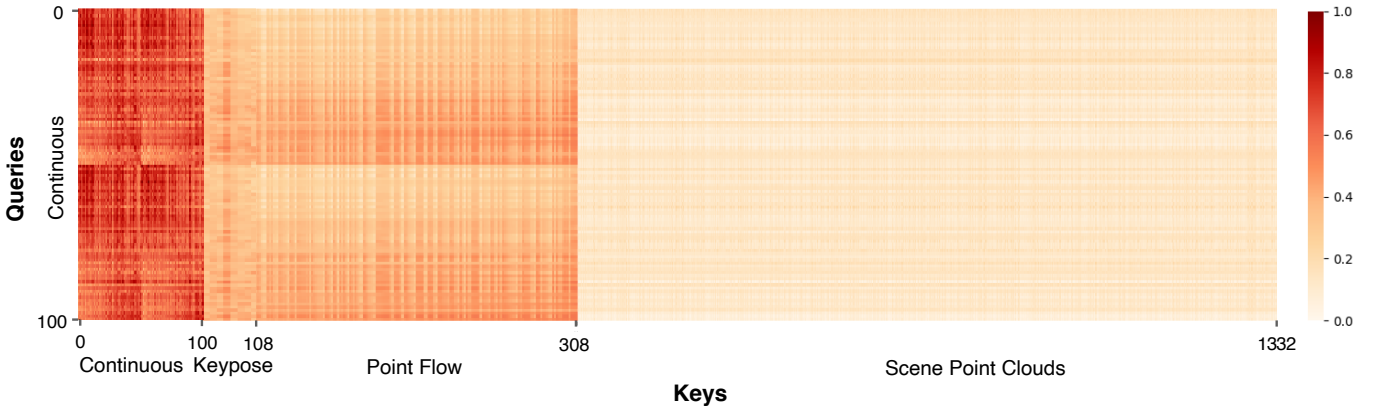


Fig. 10: **Heatmap of the attention weights of continuous action tokens.** The y-axis represents continuous action tokens as queries. The x-axis sequentially displays continuous action, keypose, pointflow, and scene tokens as keys.

focus on the tray—the key task-relevant object and disperse attention across both the tray and the robotic arm. This suggests why continuous-based policies often struggle with precise localization, as observed in previous experiments.

In contrast, as shown in the middle and right images, PPI’s pointflow and keypose tokens strongly attend to the tray, with pointflow tokens specifically concentrating on its edges—where the gripper is poised to grasp. Since the initial query points are sampled from the tray rather than the cube atop it, the model learns to deprioritize the cube. This explains why in the “Carry the Tray” task, replacing in-distribution cups with out-of-distribution Rubik’s Cubes and colorful cubes does not impair PPI’s localization performance. By strategically selecting initial query points during training, the model learns to track the overall object’s motion, improving generalization under disturbances.

Further, we examine how these interfaces guide continuous action prediction. As shown in Figure 10, continuous action tokens exhibit significantly higher attention weights toward keypose and pointflow tokens than scene tokens, underscoring the critical role of interfaces in action prediction. By incorporating target gripper poses and object pointflow as interfaces, PPI not only maintains focus on task-relevant regions despite scene variations but also alleviates the learning burden on

action tokens by distilling key information, rather than directly querying from the entire scene.

VI. CONCLUSION AND LIMITATION

We introduce PPI, an end-to-end interface-based manipulation policy that leverages target gripper poses and object pointflow. PPI achieves state-of-the-art performance on the RLBench2 simulation benchmark and demonstrates strong effectiveness and robustness in real-world experiments. However, two key limitations remain. First, the computational cost of visual foundation models and the diffusion process constrains efficiency. Future work will focus on accelerating diffusion sampling and adopting lightweight vision models. Second, cross-embodiment evaluation on different robotic platforms is essential to assess PPI’s generalization across hardware.

REFERENCES

- [1] Homanga Bharadhwaj, Roozbeh Mottaghi, Abhinav Gupta, and Shubham Tulsiani. Track2act: Predicting point tracks from internet videos enables generalizable robot manipulation. In *Arxiv*, 2024.

- [2] Jan Kautz Stan Birchfield Bowen Wen, Wei Yang. FoundationPose: Unified 6d pose estimation and tracking of novel objects. In *CVPR*, 2024.
- [3] Anthony Brohan, Noah Brown, Justice Carbajal, Yevgen Chebotar, Joseph Dabis, Chelsea Finn, Keerthana Gopalakrishnan, Karol Hausman, Alex Herzog, Jasmine Hsu, et al. Rt-1: Robotics transformer for real-world control at scale. In *Arxiv*, 2022.
- [4] Cheng Chi, Zhenjia Xu, Siyuan Feng, Eric Cousineau, Yilun Du, Benjamin Burchfiel, Russ Tedrake, and Shuran Song. Diffusion policy: Visuomotor policy learning via action diffusion. In *RSS*, 2023.
- [5] Shivin Devgon, Jeffrey Ichnowski, Ashwin Balakrishna, Harry Zhang, and Ken Goldberg. Orienting novel 3d objects using self-supervised learning of rotation transforms. In *CASE*, 2020.
- [6] Danny Driess, Fei Xia, Mehdi SM Sajjadi, Corey Lynch, Aakanksha Chowdhery, Brian Ichter, Ayzaan Wahid, Jonathan Tompson, Quan Vuong, Tianhe Yu, et al. Palm-e: An embodied multimodal language model. In *Arxiv*, 2023.
- [7] Ben Eisner, Harry Zhang, and David Held. Flowbot3d: Learning 3d articulation flow to manipulate articulated objects. In *RSS*, 2022.
- [8] Hao-Shu Fang, Chenxi Wang, Hongjie Fang, Minghao Gou, Jirong Liu, Hengxu Yan, Wenhui Liu, Yichen Xie, and Cewu Lu. Anygrasp: Robust and efficient grasp perception in spatial and temporal domains. In *TRO*, 2023.
- [9] Markus Grotz, Mohit Shridhar, Tamim Asfour, and Dieter Fox. Peract2: A perceiver actor framework for bimanual manipulation tasks. In *Arxiv*, 2024.
- [10] Jonathan Ho, Ajay Jain, and Pieter Abbeel. Denoising diffusion probabilistic models. In *NeurIPS*, 2020.
- [11] Stephen James and Andrew J. Davison. Q-attention: Enabling efficient learning for vision-based robotic manipulation. In *IEEE Robotics and Automation Letters*, 2022.
- [12] Nikita Karaev, Ignacio Rocco, Benjamin Graham, Natalia Neverova, Andrea Vedaldi, and Christian Rupprecht. Cotracker: It is better to track together. In *ECCV*, 2024.
- [13] Tsung-Wei Ke, Nikolaos Gkanatsios, and Katerina Fragkiadaki. 3d diffuser actor: Policy diffusion with 3d scene representations. In *CoRL*, 2024.
- [14] Moo Jin Kim, Karl Pertsch, Siddharth Karamcheti, Ted Xiao, Ashwin Balakrishna, Suraj Nair, Rafael Rafailov, Ethan Foster, Grace Lam, Pannag Sanketi, et al. Openvla: An open-source vision-language-action model. In *CoRL*, 2024.
- [15] Alexander Kirillov, Eric Mintun, Nikhila Ravi, Hanzi Mao, Chloe Rolland, Laura Gustafson, Tete Xiao, Spencer Whitehead, Alexander C. Berg, Wan-Yen Lo, Piotr Dollár, and Ross Girshick. Segment anything. In *Arxiv*, 2023.
- [16] I Liu, Chun Arthur, Sicheng He, Daniel Seita, and Gaurav Sukhatme. Voxact-b: Voxel-based acting and stabilizing policy for bimanual manipulation. In *CoRL*, 2024.
- [17] Shilong Liu, Zhaoyang Zeng, Tianhe Ren, Feng Li, Hao Zhang, Jie Yang, Chunyuan Li, Jianwei Yang, Hang Su, Jun Zhu, et al. Grounding dino: Marrying dino with grounded pre-training for open-set object detection. In *Arxiv*, 2023.
- [18] Songming Liu, Lingxuan Wu, Bangguo Li, Hengkai Tan, Huayu Chen, Zhengyi Wang, Ke Xu, Hang Su, and Jun Zhu. Rdt-1b: a diffusion foundation model for bimanual manipulation. In *Arxiv*, 2024.
- [19] Maxime Oquab, Timothée Darcet, Theo Moutakanni, Huy V. Vo, Marc Szafraniec, Vasil Khalidov, Pierre Fernandez, Daniel Haziza, Francisco Massa, Alaaeldin El-Nouby, Russell Howes, Po-Yao Huang, Hu Xu, Vasu Sharma, Shang-Wen Li, Wojciech Galuba, Mike Rabbat, Mido Assran, Nicolas Ballas, Gabriel Synnaeve, Ishan Misra, Herve Jegou, Julien Mairal, Patrick Labatut, Armand Joulin, and Piotr Bojanowski. Dinov2: Learning robust visual features without supervision. In *Arxiv*, 2023.
- [20] Chuer Pan, Brian Okorn, Harry Zhang, Ben Eisner, and David Held. Tax-pose: Task-specific cross-pose estimation for robot manipulation. In *CoRL*, 2023.
- [21] Ethan Perez, Florian Strub, Harm de Vries, Vincent Dumoulin, and Aaron Courville. Film: Visual reasoning with a general conditioning layer. In *Proceedings of the AAAI Conference on Artificial Intelligence*, 2017.
- [22] Carl Qi, Yilin Wu, Lifan Yu, Haoyue Liu, Bowen Jiang, Xingyu Lin, and David Held. Learning generalizable tool-use skills through trajectory generation. In *IROS*, 2024.
- [23] Charles R. Qi, Li Yi, Hao Su, and Leonidas J. Guibas. Pointnet++: Deep hierarchical feature learning on point sets in a metric space. In *Arxiv*, 2017.
- [24] Alec Radford, Jong Wook Kim, Chris Hallacy, Aditya Ramesh, Gabriel Goh, Sandhini Agarwal, Girish Sastry, Amanda Askell, Pamela Mishkin, Jack Clark, Gretchen Krueger, and Ilya Sutskever. Learning transferable visual models from natural language supervision. In *Arxiv*, 2021.
- [25] Nikhila Ravi, Valentin Gabeur, Yuan-Ting Hu, Ronghang Hu, Chaitanya Ryali, Tengyu Ma, Haitham Khedr, Roman Rädle, Chloe Rolland, Laura Gustafson, et al. Sam 2: Segment anything in images and videos. In *Arxiv*, 2024.
- [26] Daniel Seita, Yufei Wang, Sarthak J Shetty, Edward Yao Li, Zackory Erickson, and David Held. Toolflownet: Robotic manipulation with tools via predicting tool flow from point clouds. In *CoRL*, 2023.
- [27] Mohit Shridhar, Lucas Manuelli, and Dieter Fox. Perceiver-actor: A multi-task transformer for robotic manipulation. In *CoRL*, 2022.
- [28] Jiaming Song, Chenlin Meng, and Stefano Ermon. Denoising diffusion implicit models. In *Arxiv*, 2020.
- [29] Jianlin Su, Yu Lu, Shengfeng Pan, Ahmed Murtadha, Bo Wen, and Yunfeng Liu. Roformer: Enhanced trans-

- former with rotary position embedding. In *Arxiv*, 2023.
- [30] Ioan A Sucan, Mark Moll, and Lydia E Kavraki. The open motion planning library. In *IEEE Robotics & Automation Magazine*, 2012.
- [31] Balakumar Sundaralingam, Siva Kumar Sastry Hari, Adam Fishman, Caelan Garrett, Karl Van Wyk, Valts Blukis, Alexander Millane, Helen Oleynikova, Ankur Handa, Fabio Ramos, et al. Curobo: Parallelized collision-free robot motion generation. In *ICRA*, 2023.
- [32] Yang Tian, Jiyao Zhang, Zekai Yin, and Hao Dong. Robot structure prior guided temporal attention for camera-to-robot pose estimation from image sequence. In *CVPR*, 2023.
- [33] Yang Tian, Jiyao Zhang, Guowei Huang, Bin Wang, Ping Wang, Jiangmiao Pang, and Hao Dong. Robokeygen: Robot pose and joint angles estimation via diffusion-based 3d keypoint generation. In *ICRA*, 2024.
- [34] Yang Tian, Sizhe Yang, Jia Zeng, Ping Wang, Dahua Lin, Hao Dong, and Jiangmiao Pang. Predictive inverse dynamics models are scalable learners for robotic manipulation. In *ICLR*, 2025.
- [35] Chenxi Wang, Hongjie Fang, Hao-Shu Fang, and Cewu Lu. Rise: 3d perception makes real-world robot imitation simple and effective. In *IROS*, 2024.
- [36] Hanqing Wang, Jiahe Chen, Wensi Huang, Qingwei Ben, Tai Wang, Boyu Mi, Tao Huang, Siheng Zhao, Yilun Chen, Sizhe Yang, et al. Grutopia: Dream general robots in a city at scale. In *Arxiv*, 2024.
- [37] Yixuan Wang, Guang Yin, Binghao Huang, Tarik Kellestemur, Jiuguang Wang, and Yunzhu Li. Gendp: 3d semantic fields for category-level generalizable diffusion policy. In *CoRL*, 2024.
- [38] Yixuan Wang, Mingtong Zhang, Zhuoran Li, Tarik Kellestemur, Katherine Driggs-Campbell, Jiajun Wu, Li Fei-Fei, and Yunzhu Li. D³fields: Dynamic 3d descriptor fields for zero-shot generalizable rearrangement. In *CoRL*, 2024.
- [39] Bowen Wen, Jonathan Tremblay, Valts Blukis, Stephen Tyree, Thomas Müller, Alex Evans, Dieter Fox, Jan Kautz, and Stan Birchfield. Bundlesdf: Neural 6-dof tracking and 3d reconstruction of unknown objects. In *Proceedings of the IEEE/CVF Conference on Computer Vision and Pattern Recognition*, pages 606–617, 2023.
- [40] Chuan Wen, Xingyu Lin, John So, Kai Chen, Qi Dou, Yang Gao, and Pieter Abbeel. Any-point trajectory modeling for policy learning. In *RSS*, 2024.
- [41] Thomas Weng, Sujay Man Bajracharya, Yufei Wang, Khush Agrawal, and David Held. Fabricflownet: Bi-manual cloth manipulation with a flow-based policy. In *CoRL*, 2022.
- [42] Philipp Wu, Yide Shentu, Zhongke Yi, Xingyu Lin, and Pieter Abbeel. Gello: A general, low-cost, and intuitive teleoperation framework for robot manipulators. In *IROS*, 2024.
- [43] Mengda Xu, Zhenjia Xu, Yinghao Xu, Cheng Chi, Gordon Wetzstein, Manuela Veloso, and Shuran Song. Flow as the cross-domain manipulation interface. In *CoRL*, 2024.
- [44] Dongjie Yu, Hang Xu, Yizhou Chen, Yi Ren, and Jia Pan. Bikc: Keypose-conditioned consistency policy for bimanual robotic manipulation. In *Arxiv*, 2024.
- [45] Chengbo Yuan, Chuan Wen, Tong Zhang, and Yang Gao. General flow as foundation affordance for scalable robot learning. In *CoRL*, 2024.
- [46] Yanjie Ze, Gu Zhang, Kangning Zhang, Chenyuan Hu, Muhan Wang, and Huazhe Xu. 3d diffusion policy. In *RSS*, 2024.
- [47] Harry Zhang, Ben Eisner, and David Held. Flowbot++: Learning generalized articulated objects manipulation via articulation projection. In *CoRL*, 2023.
- [48] Tony Z Zhao, Vikash Kumar, Sergey Levine, and Chelsea Finn. Learning fine-grained bimanual manipulation with low-cost hardware. In *RSS*, 2023.
- [49] Yan Zhao, Ruihai Wu, Zhehuan Chen, Yourong Zhang, Qingnan Fan, Kaichun Mo, and Hao Dong. Dualafford: Learning collaborative visual affordance for dual-gripper manipulation. In *ICLR*, 2023.